ELSEVIER

PII: S0032-3861(97)10323-8

Polymer Vol. 39 No. 15, pp. 3537–3544, 1998

0032-3861/98/$19.00+0.00

Structural and morphological features of the syndiotactic polystyrene/ethylbenzene complex

Stéphane Moyses, Philippe Sonntag†, Stephen J. Spells* and Olivier Laveix‡
Materials Research Institute and Division of Applied Physics, Sheffield Hallam University, City Campus, Sheffield S1 1WB, UK
(Received 27 November 1996; revised 15 August 1997)

The δ-phase of the syndiotactic polystyrene/ethylbenzene system, as formed by crystallisation from dilute solution, is shown to result in a lamellar morphology, with a monoclinic crystal lattice similar to that already reported for the complex with toluene. Combined SAXS, *FT*i.r., d.s.c. and t.g.a. measurements show that an increase in the X-ray long period between 80 and 120°C is related to solvent loss and decomplexation. There is also some temporary loss in helical order. SANS measurements on the δ-phase reveal negligible isotopic fractionation. The small increase in the in-plane radius of gyration with increasing molecular weight is interpreted as evidence of a sheetlike molecular conformation, with superfolding at higher molecular weights leading to a multiple sheet structure. On transformation to the solvent-free γ-phase, an increase in radius of gyration results from a displacement of crystal stems out of the δ-phase sheets.

(Keywords: syndiotactic polystyrene; neutron scattering; complex)

INTRODUCTION

Following the initial synthesis of the highly stereoregular syndiotactic form of polystyrene (sPS)[1,2], this polymer has generated widespread interest. Rapid crystallisation to high levels of crystallinity and a high crystal melting temperature have contributed to this commercial interest, while the complex polymorphism[3] has led to extensive research. Polymer–solvent complexes, or clathrates, are obtained with a range of solvents[4] and involve a helical polymer structure. The solvated structure is termed the δ-phase, which transforms on heating and removal of solvent to the helical γ-phase. Further heating leads to α- or β-forms, depending on heating conditions, with planar zigzag chains in both cases[3]. Additional possible structures include superlattices to the α- and β-forms (e.g. Ref.[5]), a mesomorphic form obtained, for example, by stretching amorphous samples[6] and an 'emptied δ-form', where solvent has been removed[7].

The present work forms part of a coordinated study of morphology and chain conformation in the various crystalline phases of sPS. A range of appropriate experimental techniques have been used to elucidate the structures and to obtain details of molecular conformational changes at the phase transitions. This paper is primarily concerned with the δ-phase and the δ- to γ-phase transition. Ethylbenzene was chosen as solvent because of the clearly defined lamellar structure in the δ-phase (as will be shown here) and because of related earlier work[8]. Crystals of the sPS/ethylbenzene complex have been grown from dilute solution and characterised using transmission electron microscopy and small angle X-ray scattering (SAXS). Since the crystal structure of the sPS/ethylbenzene complex has not been published, wide-angle X-ray scattering (WAXS) was undertaken from crystal mats, with the aim of determining any differences by comparison with the published structure for the sPS/toluene complex[4]. The annealing behaviour of the δ-phase has been studied, using the long period as obtained using SAXS. In addition, we report here preliminary small-angle neutron scattering (SANS) measurements of molecular dimensions in the δ- and γ-phases.

MATERIALS

Samples of sPS and fully deuterated sPS were kindly supplied by Professor V. Vittoria (Universita di Salerno) and Dr. J.-M. Guenet (Université Louis Pasteur, Strasbourg). N.m.r. measurements confirmed tacticities in excess of 99%. G.p.c. measurements were kindly supplied by RAPRA Technology Ltd. (Shawbury, UK) and indicated values for $\bar{M}_w$ for the deuterated materials of 42 700, 124 500, 144 500 and 124 000 (samples AD, BD, CD and DD, respectively). The polydispersities were generally between 2 and 3. Values of $\bar{M}_w$ for sPS samples were 85 400 and 55 700 (samples AH and BH, respectively), with somewhat higher polydispersities.

EXPERIMENTAL DETAILS

Electron microscopy was carried out using a Philips CM20 TEM, operating at 160 kV and using a tungsten filament. A drop of the crystal suspension was deposited onto a carbon-coated electron microscope grid. The grid was allowed to dry in air before mounting in the microscope. This procedure means that the sample is in the δ-phase on introduction to the microscope, but solvent is removed on

* To whom correspondence should be addressed
† Present address: Institut fur Umweltanalytik Uni GHS, FB8 Gebaude T03 R01 C95, Universitatstrasse 3–5, D45141 Essen, Germany.
‡ Present address: Département Mesures Physiques, Institut Universitaire de Technologie, 33405 Talence, France.

Figure 1 Transmission electron micrograph of sPS crystals formed from dilute solution in ethylbenzene. The bar represents 0.40 μm

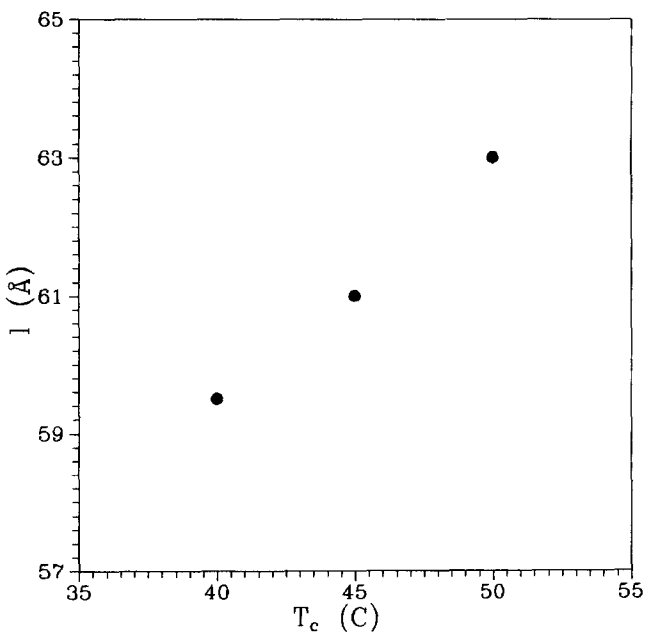

Figure 2 Long period *versus* crystallization temperature for sPS crystallised from dilute solution in ethylbenzene

Table 1 Values obtained for the unit cell parameters of sPS/ethylbenzene (final column) compared with previous values quoted for sPS/toluene[4] (middle column)

Unit cell parameters	Chatani et al.[4]	This work
a (nm)	1.76	1.77
b (nm)	1.33	1.34
c (nm)	0.77	0.80
γ (°)	121.2	121.7

application of a vacuum. Small- and wide-angle X-ray scattering were carried out on a Rigaku-Denki camera with a camera length of 316 mm and a Warhus camera with a camera length of 73 mm, respectively. In both cases Cu Kα radiation, pinhole collimation and photographic detection were used. The thermal behaviour was investigated by means of a DSC 30 and a TG 50 apparatus from Mettler. In both cases a heating rate of 10°C min^{-1} was used. Infrared spectra were obtained using a Mattson 6020 FTIR spectrometer, with an MCT detector. Measurements typically involved 200 scans and a resolution of 2 cm^{-1}. Small-angle neutron scattering (SANS) measurements were made using LOQ at the ISIS neutron source (Chilton, UK). The available range of momentum transfer $q = 4\pi \sin\theta/\lambda$ (where 2θ is the scattering angle, and λ the neutron wavelength), was from 9×10^{-3} to 2.5×10^{-1} Å^{-1}. The γ-phase samples used for neutron scattering were obtained by heating the sample previously in the δ-phase for 5 h at 135°C. WAXS confirmed that the γ-phase was attained after this heat treatment.

CRYSTALLISATION FROM ETHYLBENZENE

Samples of polymer were dissolved by heating to form 0.1% w/w solutions in ethylbenzene. The solutions were transferred to an oil bath held at the required crystallisation temperature to within 0.5°C. Filtration at room temperature, using a stack of flat horizontal filter papers, produced a mat which was allowed to dry in air. In the later stages, the mat was sandwiched between several dry filter papers, with gentle pressure applied from a glass plate. Mats obtained in this way were shown, from WAXS data, to have good c-axis orientation. Measurements of sample weight before and after heating indicated a weight loss of around 14%. For each crystallisation temperature, a small part of the crystal suspension was used for TEM samples as described above.

Figure 1 shows the characteristic lamellar morphology obtained for crystallisation at 40°C. The vacuum in the TEM sample chamber removes solvent from the crystals, but it is believed that the observed features are still characteristic of the δ-phase. The formation of lamellar stacks is typical, with widespread Moiré fringes indicative of dislocation networks. It was found to be difficult to observe individual single crystals, in part because of extensive twinning. For a crystallisation temperature (T_c) of 50°C, a change to a more fibrous morphology was observed. For this reason, later experiments involved only a crystallisation temperature of 40°C.

Figure 2 shows the variation of the X-ray long period (l_x) with T_c. Although the magnitude of the change is small, the observed increase in l_x with increasing T_c is consistent with the behaviour normally observed for crystalline polymers.

SPS/ETHYLBENZENE CRYSTAL STRUCTURE

The sPS/toluene complex has been shown to have a monoclinic $P2_{1/a}$ structure, with the parameters listed in *Table 1*[4]. Although our solution-grown crystals were shown to be well oriented within the mat, they are not ideal for this characterization in comparison to uniaxially oriented fibres, as used by Chatani *et al.*[4]. No evidence was found for departures from a monoclinic structure, and the unit cell parameters were refined on this basis. The cell parameters obtained in this way for sPS/ethylbenzene showed only

minor differences compared with those reported for sPS/toluene.

The γ-phase has been indexed by Chatani *et al.*[4] in terms of a monoclinic structure. Our data are consistent with data presented earlier, in that the *b* dimension shrinks by about 1.6 Å[4,8] upon transition from the δ- to the γ-phase, while the *a* and *c* dimensions remain approximately constant.

SAXS LONG PERIOD, INFRARED AND THERMAL MEASUREMENTS

A combination of SAXS, *FT*i.r., d.s.c. and t.g.a. measurements allowed us to correlate the specific information provided by each of these techniques, namely long period, amount of helical content, thermal events and solvent content.

We heated a piece of mat initially in the δ-phase from room temperature to T_a, by steps of 10°C, T_a ranging from 80 to 170°C. The rate of heating was 10°C min^{-1}. After reaching T_a, the sample was cooled to room temperature and analysed by SAXS and infrared spectroscopy before heating from the previous T_a to the next value. Another set of SAXS experiments consisted of heating a piece of mat for 30 min at a given temperature before recording the SAXS pattern at room temperature. D.s.c. and t.g.a. were carried out using the same heating rate (10°C min^{-1}). The 934 and 943 cm^{-1} infrared bands have been assigned to the helical conformation of the chains[9]. After normalisation of the spectrum using the 1585 cm^{-1} benzene ring stretching vibration[9], the area of the doublet was measured and plotted as a function of the annealing temperature.

Results are shown in *Figure 3*. The long period, initially 59 Å, starts increasing at about 80°C. This increase

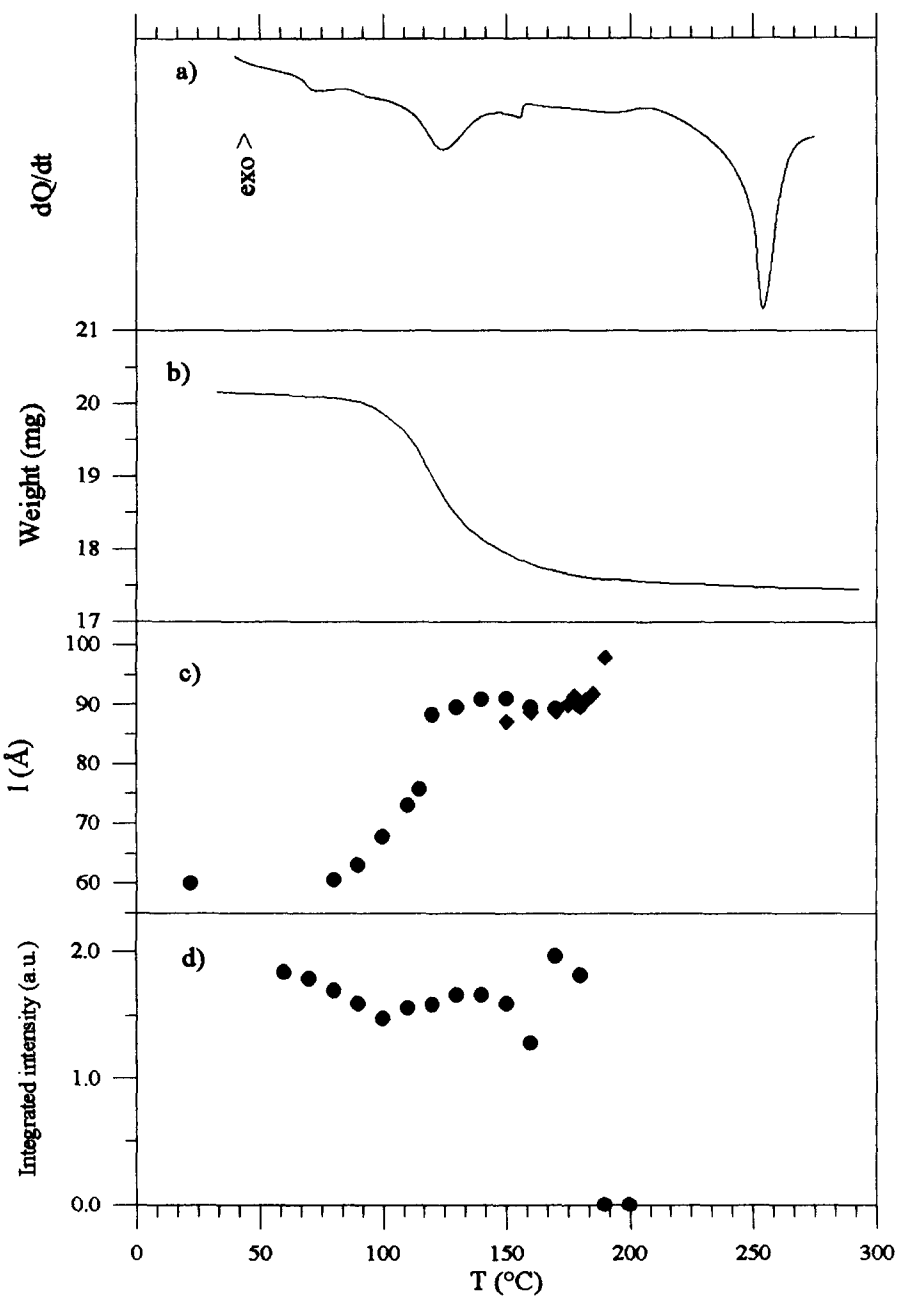

Figure 3 (a) D.s.c. and (b) t.g.a. plots for a sample initially in the δ-phase. (c) Long period *versus* annealing temperature for solution-crystallised mats: ●, annealing time 15 s; ◆, annealing time 30 min. (d) Integrated intensity of the 934/942-cm^{-1} infrared doublet assigned to the helical conformation. In all cases the heating rate was 10°C min^{-1}

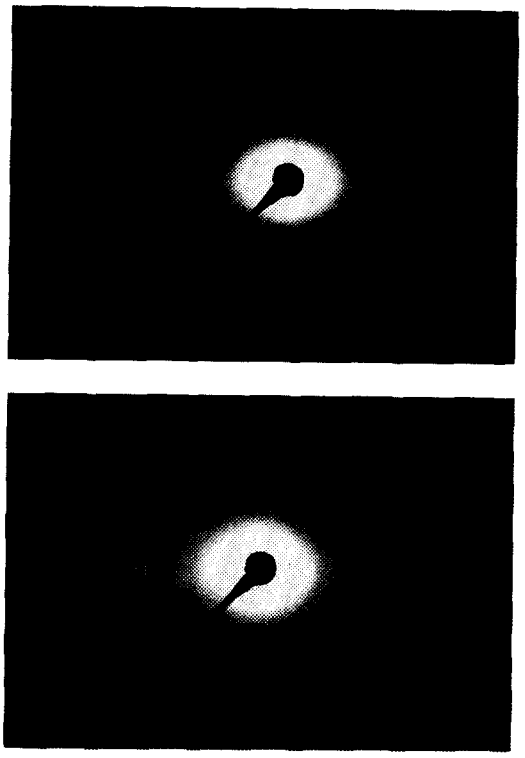

Figure 4 SAXS patterns from δ-phase (top) and γ-phase (bottom) samples of sPS. Strips of sample mats were mounted 'edge-on' to the X-ray beam

continues up to around 120°C, after which the thickness remains constant up to 180°C, and then increases again. The d.s.c. plot shows many events which have previously been described elsewhere. The feature at 71.5°C appears to be the glass transition, albeit at a somewhat lower value than has been reported[9]. Peaks observed at 123.6, 158.5, 193.0, 208.0 and 253.3°C are identified with δ to γ transition, recrystallization of γ, γ to α transition (slow heating rate[10]), recrystallisation of α[10] and melting of α, respectively. From the t.g.a. plot, it can be seen that the solvent is expelled from the polymer in the region between 90 and 170°C.

It is well known that annealing generally results in the thickening of polymer crystals. The region of increasing long period (*Figure 3c*) between 80 and 120°C corresponds to the major region of weight loss in t.g.a. experiments (*Figure 3b*), which can in turn be related to the d.s.c. transition from the δ- to the γ-phase (*Figure 3a*). We therefore identify the change with lamellar thickening accompanying the decomplexation. *Figure 4* shows SAXS patterns obtained for both δ- and γ-phase samples. These demonstrate the degree of orientation achieved with sedimented mats and show no significant loss in crystal orientation at the phase transition.

Infrared measurements show that the helical conformation is partly disordered at the earliest stage of the transition and finally returns to a value close to its initial value. Thus, there is no overall increase in the helical content upon transition from δ-phase to the γ-phase, and the thickening cannot be explained by crystallization of amorphous material. According to t.g.a., the majority of solvent molecules is still present when the amount of chains in the helical conformation has decreased to its minimum at 100°C. This disordered state is temporary: as the temperature rises, the solvent molecules are expelled and the conformational order of the chain increases to return to its initial value while the long period is increasing. The helical content and the long period reach their plateau together. We suggest that these observations can only be reconciled by a mechanism of lamellar thickening involving no change in crystallinity. Such a process would be facilitated by a large proportion (≈ 25%) of crystal defects throughout the δ to γ transition. This proportion of defects cannot directly explain the increase in lamellar thickness, since even the formation of fully extended planar zigzag sequences would not produce such a large thickening. Rather, the presence of solvent molecules appears to promote thickening in a similar way to that observed for suspensions of polymer crystals in solvent[11], and the motion of defects is presumably also involved. The interpretation of the d.s.c. peak at 158.5°C as being due to the recrystallization is confirmed by infrared measurements, which show a sudden increase in helical content at this temperature. The helix structure vanishes as the temperature of the γ to α transition is reached, and the chains adopt the planar zigzag conformation, leading to a further increase of the long period.

The transition from the γ-phase to the α-phase occurs with a significant change in long period. There are two possible explanations for this thickening in addition to lamellar thickening generally observed on approaching the melting temperature. First, the γ- to α-phase transition appears to be followed immediately by recrystallisation (*Figure 3a*). Second, the transition involves a change in molecular conformation from helical to planar zigzag. Both phenomena may result in changes of long period, in the first case through the transformation of amorphous material into the crystalline state, and in the second through a decrease in the number of monomers per unit length of stem of about 25%, and as a result in an overall increase of the chain extension within the crystal.

As previously mentioned, the γ-phase samples used for neutron scattering were obtained by fast heating in comparison to the relatively slow heating (10°C min^{-1}) used before. For these samples, the measured long periods are significantly smaller (73 Å) than the value obtained at 135°C from *Figure 3* of about 92 Å. Dependence of the long period on the heating rate, as well as the annealing temperature, has previously been noted for polyethylene[12], and the behaviour here is consistent with a delay in the thickening process for high heating rates in comparison to slower heating rates.

SANS MEASUREMENTS OF CHAIN CONFORMATION

Results presented below are part of a wider neutron scattering study of molecular conformations in sPS. In a following paper[13] we will present intermediate-angle scattering data in conjunction with model calculations using statistical arrangements of crystal 'stems' (the segments of polymer which traverse the lamella).

Samples consisted of a protonated sPS matrix and 5% (w/w) of deuterated sPS as labelled molecules. As a consequence of sample availability, two series of samples were prepared differing in the protonated matrix. Also, it was not possible to match the molecular weight of the protonated and deuterated molecules in order to give identical melting temperatures. This difference and the resulting fractional crystallization may give rise to: (i) isotopic fractionation ('segregation'), and (ii) molecular weight fractionation. The first of these effects can be

detected using an extrapolation to zero angle from SANS data. The second may give rise to label concentrations which differ from their initial values (5%). In order to verify this, and to carry out the blank subtractions, real isotopic concentrations need to be known. We used infrared spectroscopy, with two standard samples of known isotopic concentration. For this purpose, mixtures of isotopic species were weighed and dissolved in toluene before casting onto KBr plates which were then heated for 30 min at 130°C in order to remove the solvent bands. Nyquist *et al.*[14] have assigned the 2849-cm^{-1} band to backbone C–H stretching modes ($\upsilon_{sym.}CH_2$). Similarly, we have assigned the 2193 cm^{-1} band to backbone C–D stretching ($\upsilon_{asym.}CD_2$). The ratio of the integrated intensities was measured, and the corresponding concentrations were calculated using the calibration curve. These results (see *Table 2*) show a small amount of fractionation by molecular weight.

Table 2 Molecular weights of the protonated and deuterated polymer as measured by GPC, and concentration of deuterated species after crystallization

Matrix	Sample	DsPS conc. (%)		Initial molecular weight ($\times 10^{-3}\bar{M}_w$) of:	
		Initial	Final	DsPS	HsPS
AH	AD	5	4.6	42.7	85.4
	BD	5	5.9	124.5	85.4
	CD	5	5.2	144.5	85.4
BH	AD	5	4.9	42.7	55.7
	BD	5	6.1	124.5	55.7
	CD	5	7.6	144.5	55.7
	DD	5	7.7	124.0	55.7

In the Guinier range, $\bar{M}_w$ and the in plane-radius of gyration R_g of the oriented mat were determined, using Zimm plots ($1/I(q)$ *versus* q^2), from the extrapolated intercept at $q = 0$ and the slope at small q, respectively. *Figure 5* shows two typical sample Zimm plots for the δ- and γ-phases with the extrapolation to zero angle. The very

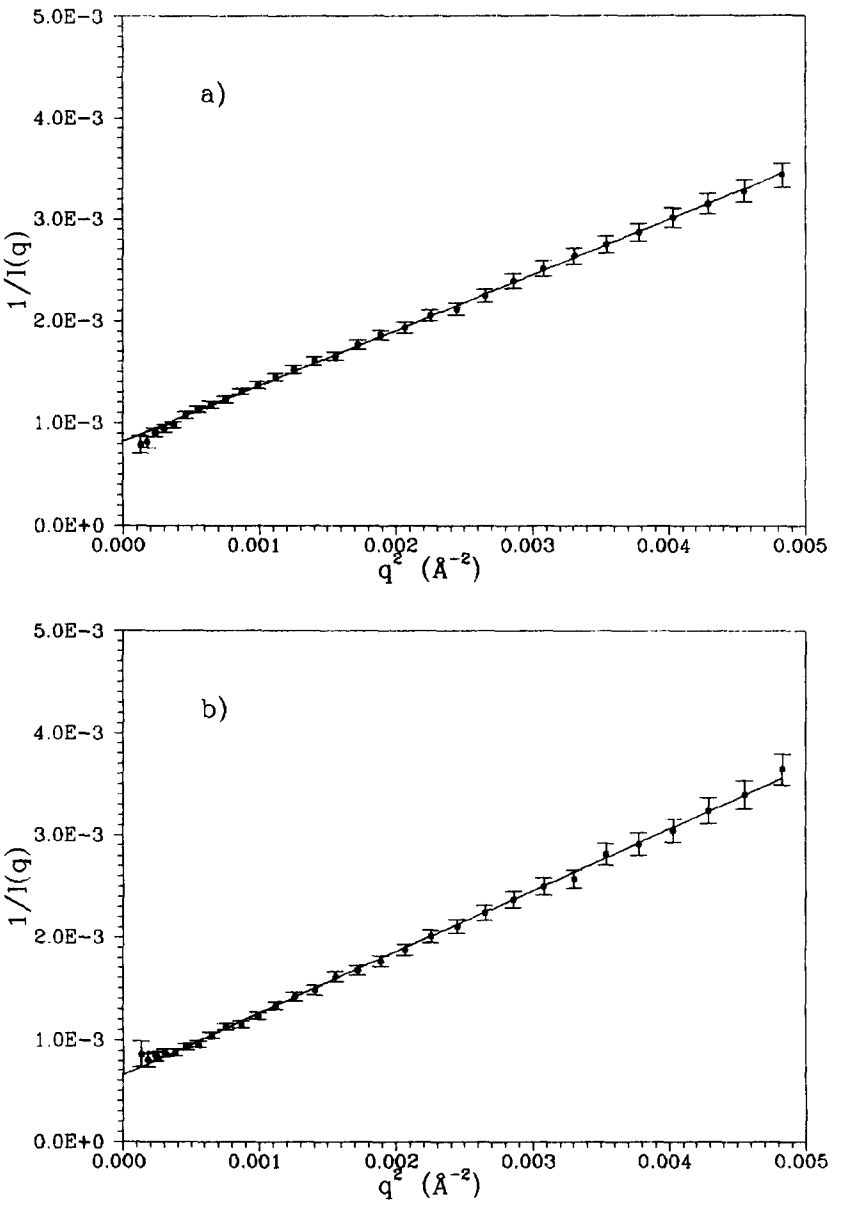

Figure 5 Typical Zimm plots for the δ-phase (top) and γ-phase (bottom) ($\bar{M}_w = 42\,700$). Data obtained using the LOQ instrument at ISIS

small excess intensity for the δ-phase sample at smallest angles indicates negligible isotopic fractionation, this conclusion being reinforced by the reasonable correlation between molecular weights, as measured by neutron scattering and g.p.c. (see *Table 3*). Measured molecular weights are somewhat low in comparison to g.p.c. values.

Table 3 Molecular weights and radii of gyration as measured by SANS

	δ		γ	
Sample/matrix	$\bar{M}_w$	R_g (Å)	$\bar{M}_w$	R_g (Å)
AD/AH	20000	45.1 ± 0.4	21000	52.0 ± 0.5
BD/AH	44000	79 ± 2	55000	97 ± 2
CD/AH	32000	68.6 ± 0.7	40000	81 ± 1
AD/BH	21000	51.6 ± 0.5	—	—
BD/BH	32000	72 ± 2	—	—
DD/BH	48000	60.8 ± 1.0	77000	85 ± 1

Such a feature, although to a lesser extent, has been reported by Sadler for polyethylene with high molecular weight[15]. Molecular weight distributions here are somewhat broader, which may explain this observation.

In *Figure 6*, the radius of gyration is plotted against the molecular weight. It can be seen that there is a small change in R_g with increasing molecular weight. We calculated, by means of a least-squares fit, the exponent α in the relationship $R_g \propto M^{\alpha}$ and obtained values of 0.31 ± 0.06 and 0.41 ± 0.09 for the δ- and γ-phases, respectively. The expected value for a random coil or an uncorrelated array of stems is 0.5. For polyethylene crystallised from solution, this exponent was found to be 0.1[16]. This result was explained by the 'superfolded sheet' model, whereby sheets of stems along the preferred crystallographic fold direction are folded back to form a stack of sheets. The value we found may represent an average of the values corresponding to two types of chain conformation: the single sheet

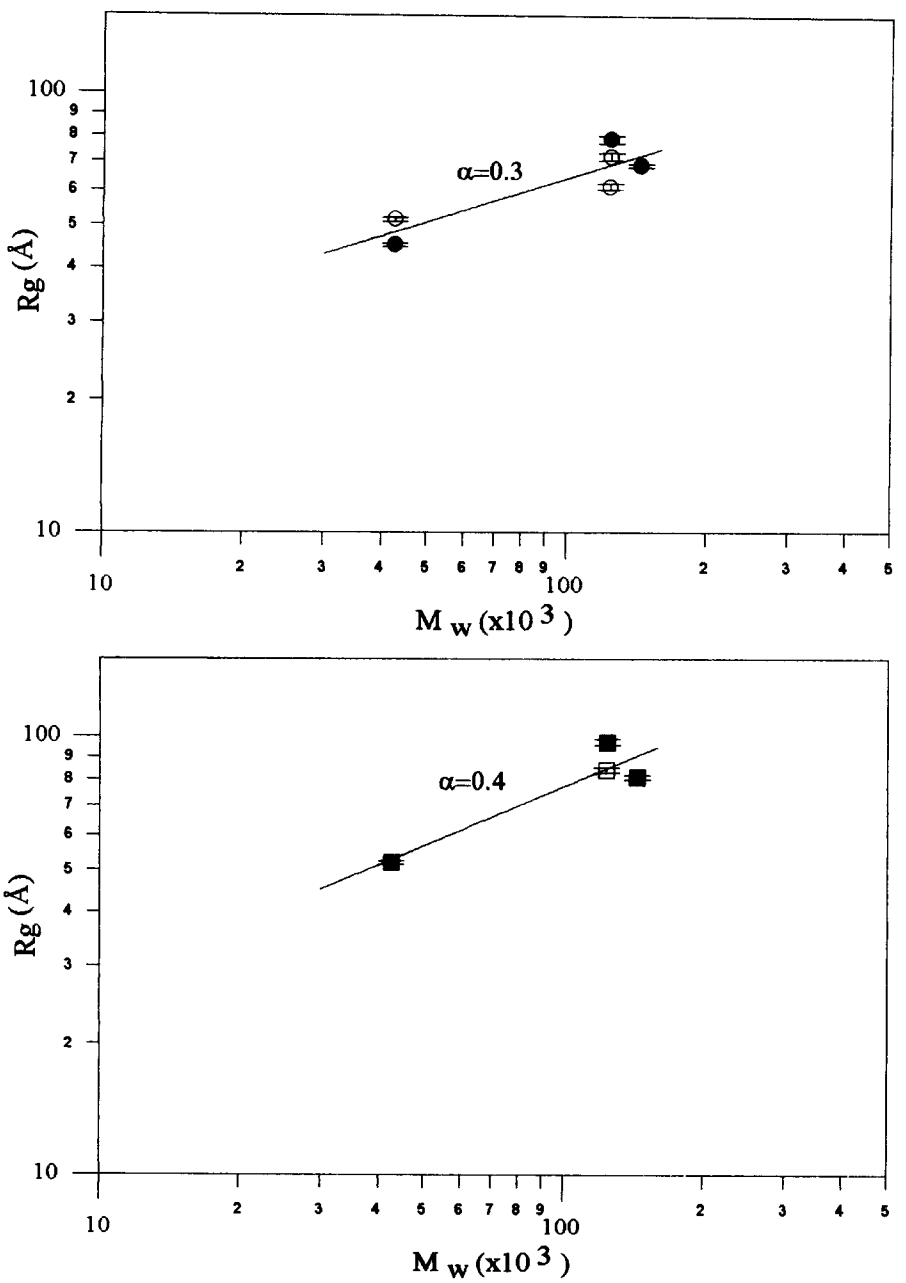

Figure 6 Radius of gyration *versus* molecular weight for δ-phase (top) and γ-phase (bottom) samples of sPS presented on a log/log plot and corresponding power fits. ●, sample in δ-phase with AH matrix; and ○, BH matrix; ■, sample in γ-phase with AH matrix; and □, BH matrix

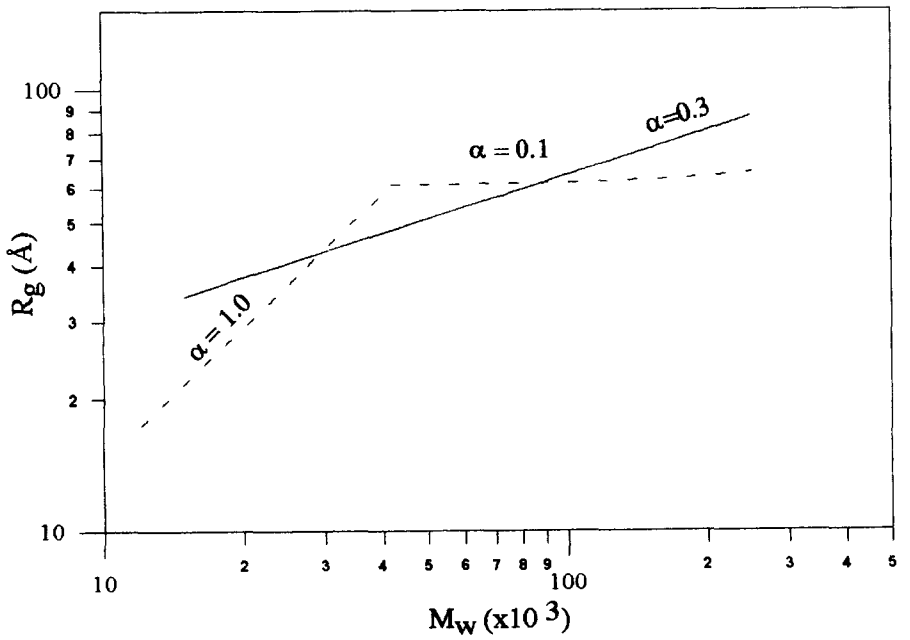

Figure 7 Radius of gyration *versus* molecular weight as calculated using equations (1) and (2) (- - -) presented with the power fit obtained for the δ-phase (——)

structure (for lowest molecular weight $\alpha \rightarrow 1$) and the multiple sheet structure (highest molecular weights $\alpha \rightarrow 0.1$). Thus the data obtained within this molecular weight range are consistent with a transition from the single sheet to the multiple sheet structure. Further support for this model will be shown from IANS data[13].

In order to illustrate this change of regime, we calculated the in-plane radius of gyration for N_r stems in one sheet in the case of purely adjacent folding[17]:

$$R_g^2 = \frac{N_r}{12} I_{\parallel}^2 \quad (1)$$

where $N_r = (\overline{M}_w)/(M_r)$. We assume here that the sample is fully crystalline and that chain folds form a negligible fraction of the molecular length. M_r is the molecular weight of the stem deduced from the thickness of the monocrystal. When superfolding occurs, the molecule folds in N_s sheets, each of them containing $N_{r/s}$ stems. In the case where the stems are placed on a rectangular lattice, R_g can be written

$$R_g^2 = \frac{N_{r/s}^2}{12} I_{\parallel}^2 + \frac{N_s^2}{12} I_{\perp}^2 \quad (2)$$

$I_{\parallel}$ and $I_{\perp}$ are, respectively, the fold and superfold lengths. We have made the assumption here that $I_{\parallel}$ and $I_{\perp}$ are large in comparison to the stem width. Chatani *et al.*[3] have suggested that folding occurs along the direction *a*, and we will confirm this result in a following paper[13]. In order to take account of the dilution of stems, instead of $I_{\parallel}$ we use *d*, the average distance between two consecutive stems in a sheet[13]. Lines representing equations (1) and (2) are plotted in *Figure 7* for a fixed number of stems per sheet equal to 12, together with the fit obtained from the experimental data for the δ-phase. This figure illustrates how a change of regime within the molecular weight range used as described above would be consistent with the measured values for the radius of gyration and the calculated exponent.

In the γ-phase, an increase of R_g is obtained (*Table 3*). It should be noted that measurements of the X-ray long period show an increase on transformation to the γ-phase, while there is no indication of any loss of crystal orientation. The fact that R_g increases at the δ to γ transition has implications for the mechanism of thickening discussed earlier: the chain reorganisation must occur on a local level, rather than on a molecular scale in order to prevent a decrease in R_g. This proposal is reminiscent of the solid-state diffusion proposed for polyethylene single crystals at low heating rates[18]. The magnitude of the increase in R_g suggests significant movement of stems upon transition. This is further supported by the increase in the α exponent indicating a more random distribution of the stems (cf. $\alpha = 0.5$ for an uncorrelated array of stems). For a simple model where stems are allowed to move only in a direction perpendicular to the sheet plane, the relation between the radius of gyration before and after displacement is:

$$R_g^{\gamma^2} = R_g^{\delta^2} + \langle \delta_{\perp}^2 \rangle \quad (3)$$

where,

$$\langle \delta_{\perp}^2 \rangle = \frac{1}{N_r} \sum_{i=1}^{N_r} \delta_i^2$$

and δ_i is the displacement length of the stem *i*.

If we apply this formula to our experimental data we find that the root mean square of the displacement length ranges from 25 to 57 Å depending on the molecular weight. This demonstrates the mobility of stems, arising from the expulsion of solvent molecules which form part of the δ-phase polymer/solvent complex. Again, this mobility is likely to be facilitated by significant numbers of crystal defects in the transition region. A molten zone of a size at least equal to molecular dimensions would give rise to fractionation of isotopic species. This is not observed, as the Zimm plots for the γ-phase samples do not show any excess intensity at small *q* (see *Figure 5*). Similarly, the low-angle intercepts are of very similar magnitudes, suggesting minimal isotopic fractionation. Thus, the regions of enhanced mobility are smaller than molecular dimensions.

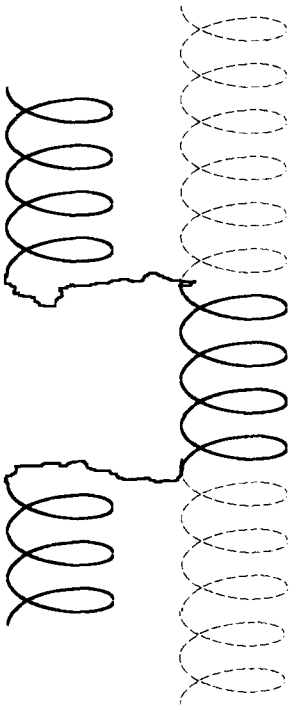

Figure 8 Proposed intermediate structure formed during the δ- to γ-phase transition. Disordered chain segments allow the movement of part of the original helix. The final stem structure, with disorder replaced by helical segments, is shown by the dashed line

CONCLUSIONS

We have demonstrated that crystallisation of sPS from dilute solution in ethylbenzene leads to the formation of lamellar crystals of the sPS/ethylbenzene complex (δ-phase). WAXS data from the mats formed are consistent with a monoclinic crystal structure, with similar unit cell parameters to those reported for the sPS/toluene complex by Chatani *et al.*[4]. The γ-phase, formed by heating the δ-phase mats, is characterised by a reduction in the cell *b* dimension.

A combination of SAXS, d.s.c. and t.g.a. measurements leads to the conclusion that the increase in long period over the temperature range from 80 to 120°C is related to decomplexation and formation of the γ-phase, with lamellar thickening promoted by the presence of solvent molecules. *FT*i.r. measurements indicate a loss of around 25% in helical order through the transition, with the helical content regained on completion of the transition. A further increase in long period above 180°C is associated with conventional lamellar thickening.

SANS measurements on the δ-phase complex are characterised by negligible isotopic fractionation, but significant fractionation by molecular weight. In-plane radius of gyration data for oriented mats show only a small increase with increasing molecular weight. The interpretation is that the structure closely resembles those already determined for non-complexing polymer/solvent systems after crystallisation from dilute solution, namely a sheetlike structure, with crystal stems arranged in a preferred crystallographic direction. This direction is shown elsewhere to be the *a* direction[13]. Furthermore, superfolding (characterised by parallel sheets of stems) occurs, as in single-crystal mats of polyethylene[20] and isotactic polystyrene[21]. This is, to our knowledge, the first time that such a structure has been observed in a polymer/solvent complex. The detailed arrangement of labelled stems within the sheets will be analysed elsewhere[13].

An increase in the radius of gyration with decomplexation and formation of the γ-phase is interpreted as evidence of the movement of crystal stems from the δ-phase sheets. A simple calculation shows this displacement to be of the order of 25–57 Å, depending on molecular weight. The formation of the γ-phase structure through the existence of zones of mobile material suggests that these zones are considerably smaller than individual molecules, since there is no evidence of enhanced isotopic fractionation.

We suggest that the movement of crystal stems is facilitated by the formation of disordered segments during the transition. This would enable helical sections of stems to move out of their original positions (*Figure 8*). Simultaneously, the presence of solvent molecules provides sufficient chain mobility for lamellar thickening. Finally, removal of most of the defects would be correspond to movement of the complete stem.

ACKNOWLEDGEMENTS

We wish to thank Dr. S.M. King (ISIS, CLRC, UK) for assistance with neutron scattering measurements, Dr. G. Ungar (University of Sheffield) for the use of SAXS facilities and Dr. J.-M. Guenet (Université Louis Pasteur, Strasbourg) for use of the differential scanning calorimeter. We would also like to thank Mr. G. Gregory for help with electron microscopy and Mr. D. Phipps for assistance with t.g.a. measurements. Support for P.S. from the E.C. Human Capital and Mobility Network, contract number ERB-CHRX-CT93-0146 is acknowledged.

REFERENCES

1. Ishihara, N., Seimiya, T., Kuramoto, M. and Uoi, M., *Macromolecules*, 1986, **19**, 2464.
2. Pellachia, C., Longo, P., Grassi, A., Ammendola, P. and Zambelli, A., *Makromol. Chem., Rapid Commun.*, 1987, **8**, 277.
3. Chatani, Y., Shimane, Y., Inoue, Y., Inagaki, T., Ishioka, T., Ijitsu, T. and Yukinari, T., *Polymer*, 1992, **33**, 488.
4. Chatani, Y., Shimane, Y., Inagaki, T., Ijitsu, T., Yukinari, T. and Shikuma, H., *Polymer*, 1993, **34**, 1620.
5. Greis, O., Xu, Y., Asano, T. and Petermann, J., *Polymer*, 1989, **30**, 590.
6. de Candia, F., Filho, A.R. and Vittoria, V., *Makromol. Chem., Rapid Commun.*, 1991, **12**, 295.
7. Manfredi, C., de Rosa, C., Guerra, G., Rapacciuolo, M., Auriemma, F. and Corradini, P., *Macromol. Chem. Phys.*, 1995, **196**, 2795.
8. Wang, Y.K., Savage, J.D., Young, D. and Hsu, S.L., *Macromolecules*, 1992, **25**, 3659.
9. Reynolds, N.M., Stidham, H.D. and Hsu, S.L., *Macromolecules*, 1991, **24**, 3662.
10. Guerra, G., Vitagliano, V.M., De Rosa, C., Petraccone, V. and Corradini, P., *Macromolecules*, 1990, **23**, 1539.
11. Magill, J.H., Girolamo, M. and Keller, A., *Polymer*, 1981, **22**, 43.
12. Spells, S.J. and Hill, M.J., *Polymer*, 1991, **32**, 2716.
13. Moyses, S. and Spells, S. J., *Polymer* (in press, accompanying paper).
14. Nyquist, R.A., Putzig, C.L., Leugers, M.A., McLachlan, R.D. and Thill, B., *Appl. Spectrosc.*, 1992, **46**, 981.
15. Sadler, D.M., *Polym. Commun.*, 1985, **26**, 210.
16. Sadler, D.M. and Keller, A., *Science*, 1979, **203**, 263.
17. Guenet, J.M. and Picot, C., *Polymer*, 1979, **20**, 1482.
18. Sadler, D.M. and Spells, S.J., *Macromolecules*, 1989, **22**, 3941.
19. Guenet, J.M., Sadler, D.M. and Spells, S.J., *Polymer*, 1990, **31**, 195.
20. Spells, S.J., Keller, A. and Sadler, D.M., *Polymer*, 1984, **25**, 749.